Atomic vibrational density of states of crystalline β-$FeSi_2$ and amorphous $FeSi_2$ thin films

M. Walterfang, W. Keune,* E. Schuster, A. T. Zayak, and P. Entel
Institute of Physics, University Duisburg-Essen, D-47048 Duisburg, Germany

W. Sturhahn, T. S. Toellner, and E. E. Alp
Advanced Photon Source, Argonne National Laboratory, Argonne, Illinois 60439, USA

P. T. Jochym and K. Parlinski
Institute of Nuclear Physics, Polish Academy of Sciences, Radzikowskiego 152, 31-342 Cracow, Poland
(Received 7 August 2004; published 11 January 2005)

Nuclear resonant inelastic x-ray scattering of 14.4125 keV synchrotron radiation was used to measure directly the partial vibrational density of states (VDOS), $g(E)$, of crystalline β-$^{57}FeSi_2$ and amorphous (a-)$^{57}FeSi_2$ thin films prepared by codeposition in ultrahigh vacuum. The structure of the samples was characterized by x-ray diffraction and Mössbauer spectroscopy. The VDOS of β-$FeSi_2$ extends up to $E_{max} \sim 65$ meV and exhibits a strong peak at $E \sim 36$ meV and weaker bands centered at about 25, 43, and 53 meV. These characteristic features coincide with positions of prominent IR and Raman spectral lines reported in the literature. The measured VDOS shows good agremeent with the theoretical VDOS of crystalline β-$FeSi_2$ computed by using the density functional theory combined with the direct method. Contrary to the crystalline phase, the VDOS of a-$FeSi_2$ shows a broad peak at ~ 30 meV with little structure, and a deviation from Debye behavior at small excitation energies (<15 meV). This is revealed as a peak in the reduced VDOS, $g(E)/E^2$, at $E_{bp} \sim 10$ meV, which is interpreted as "boson peak." Above the boson peak ($30\ \text{meV} \lesssim E \lesssim 60\ \text{meV}$) $g(E)/E^2$ was observed to be approximately $\propto \exp(-E/E_0)$, with $E_0 = 7.4$ meV being close to E_{bp}.

DOI: 10.1103/PhysRevB.71.035309 PACS number(s): 61.10.Eq, 63.22.+m, 63.50.+x, 76.80.+y

I. INTRODUCTION

The semiconducting crystalline iron-disilicide β-$FeSi_2$ is of technological interest as a potential candidate for applications in optoelectronics and thermoelectric silicon-compatible devices.[1] β-$FeSi_2$ exhibits a direct band gap of 0.83–0.87 eV[2,3] at RT, which is within the absorption minimum of optical fibers. A light emitting diode of β-$FeSi_2$ precipitates in silicon was successfully fabricated.[4] More recently, semiconducting amorphous iron-disilicide (a-$FeSi_2$) with a direct band gap of 0.88 eV was successfully synthesized by ion-beam mixing,[5] offering potential applications in large-area electronics.

From a fundamental point of view, β-$FeSi_2$ is an interesting material, since it displays a Jahn-Teller-like phase transition from the metastable CaF_2-type metallic γ-$FeSi_2$ structure to the stable orthorhombic semiconducting β-$FeSi_2$ phase, involving moderate lattice distortions of the fluorite structure.[6] γ-$FeSi_2$ can be stabilized epitaxially at very low film thickness on Si(111),[6–10] but a structural transition to β-$FeSi_2$ occurs by increasing the thickness. Theoretical work has shown that this structural transformation is promoted by the high electron density of states at the Fermi level of γ-$FeSi_2$ and strong electron-phonon coupling,[6] resulting in phonon instabilities in γ-$FeSi_2$. Although phonon dispersion curves and phonon (or vibrational) density of states (VDOS) of the metastable fluorite phase have been calculated,[6] it is surprising that to the best of our knowledge, no literature reports (neither theoretical nor experimental) exist on the VDOS of the stable β-$FeSi_2$ phase, and for amorphous $FeSi_2$ as well. The purpose of our present work is to fill this gap. Further, it is interesting to compare the VDOS of the crystalline and amorphous $FeSi_2$ phases and reveal modifications induced by the amorphous structure. Amorphous systems are expected to exhibit anomalous behavior in the low-energy part of the VDOS, $g(E)$. In particular, amorphous and disordered materials display an excess of low-energy modes compared to the usual Debye-type E^2 law of the crystalline behavior.[11,12] Inelastic neutron scattering has revealed the existence of such excess vibrational modes in different materials,[13,14] the so-called "boson peak." The origin of the boson peak is still a matter of debate.[15–20]

Nuclear resonant inelastic x-ray scattering (NRIXS) of synchrotron radiation by Mössbauer nuclei is a method to explore atomic vibrational properties of condensed matter not available otherwise.[21–26] It gives direct access to the energy distribution of atomic vibrations, i.e., the VDOS for the vibrating resonant isotope in matter. In other words, it is the resonant-isotope projected "partial" VDOS that is directly measured by NRIXS. Thus, NRIXS is complementary to other relevant methods as inelastic neutron, inelastic x-ray and Raman scattering, which mainly deal with phonon dispersion relations. Because of the high cross section for nuclear resonant scattering NRIXS may be applied for studying the vibrational properties of crystalline or amorphous thin films and multilayers.[27–30] The VDOS is a key quantity from which important thermodynamic properties may be deduced. Recent reviews of the NRIXS method are given in Refs. 24, 25, and 31.

II. EXPERIMENT

For the preparation of crystalline β-$FeSi_2$ films a Si(100) wafer was initially cleaned with 10% HF solution and then

heated at 650 °C for 10 min under UHV conditions (base pressure 5×10^{-9} mbar) to remove the surface contaminants, before depositing a 60-Å-thick ^{nat}Fe buffer layer of natural isotopic abundance (of ~2% ^{57}Fe) at RT. After *in situ* annealing in UHV at 700 °C for 3 h a pure β-$FeSi_2$ layer was formed. This deposition mode is known as solid phase epitaxy.[32,33] Then a 3000-Å-thick β-$FeSi_2$ layer was grown at 500 °C by stoichiometric coevaporation of ^{57}Fe (99.95 at. % purity, 95.5% enriched in ^{57}Fe) and Si 99.999 at. % purity) (pressure during growth: 5×10^{-9} mbar). Subsequently the sample was *in situ* annealed in UHV at 700 °C for 3 h.

A 3000-Å-thick amorphous $FeSi_2$ layer was quench-condensed in UHV by stoichiometric coevaporation of ^{57}Fe (99.95 at. % purity, 95.5% enriched in ^{57}Fe) and Si (99.999 at. % purity) on a $Al_2O_3(11\bar{2}0)$ (sapphire) substrate held at RT. The sapphire substrate was previously heated in UHV at 650 °C for 10 min to remove surface contaminants. For all samples, ^{nat}Fe and ^{57}Fe were evaporated from alumina crucibles in homemade Knudsen cells, and Si from an electron gun. The deposition rates of ^{57}Fe (0.1 Å/s) and Si (0.34 Å/s) and the film thicknesses were measured by two independent calibrated quartz crystal oscillators and controlled by a personal computer.

The structure of the samples was characterized ex-situ by (θ-2θ) x-ray diffraction (XRD) and ^{57}Fe conversion electron Mössbauer spectroscopy (CEMS). Cu K_α radiation and a graphite monochromator were used for XRD. CEM spectra were taken at RT by placing the sample inside of a conventional He-CH_4 proportional counter with the film surface perpendicular to the incident 14.4 keV γ-ray of the ^{57}Co source (Rh matrix). The CEM spectra were least-squares fitted by using the NORMOS computer program by Brand.[34] Isomer shift (δ) values are given relative to a α-Fe absorber at RT.

The NRIXS experiments were performed at RT at the undulator beamline 3-ID of the Advanced Photon Source in Argonne (USA). The method of inelastic nuclear resonant absorption of 14.4125 keV x rays is selective to the ^{57}Fe resonant isotope and provides the Fe-projected (partial) VDOS rather directly with a minimum of modeling.[22,25] Details of the technique are described elsewhere.[21–25] The monochromatized synchrotron radiation was incident onto the film surface under a grazing angle of ~4 mrad and had an energy bandwidth [full width at half maximum (FWHM)] of 1 meV. The X-ray beam was focused to about 10×10 μm^2 in size. The energy was tuned around the 14.4125 keV nuclear resonance of ^{57}Fe. The NRIXS data evaluation and extraction of the VDOS were performed by using the computer program PHOENIX described elsewhere.[35] The thickness of 3000 Å of our β-$FeSi_2$ and a-$FeSi_2$ films is sufficiently large, so that their measured VDOS distributions are representative of the bulk materials.[28–30]

III. THEORY

The present *ab initio* calculations of β-$FeSi_2$ were performed within the density functional theory, using VASP package[36,37] and the generalized gradient approximation (GGA). The Vanderbilt-type ultrasoft pseudopotentials,[38] provided with the package, were used for Fe and Si atoms. We have used a 48 atomic supercell identical with the crystallographic unit cell with *Cmca* space group symmetry. The Brillouin zone integration was confined to Γ wavevectors. The optimized lattice constants are: $a=9.7677$ Å, $b=7.8140$ Å, and $c=7.8652$ Å. The Fe and Si atoms were considered as magnetic ions, but the resulting magnetic moments were zero.

The lattice dynamics calculations were carried out within the direct method,[39,40] using the 48 atomic supercell. For that the Hellmann-Feynman forces were computed for positive and negative displacements with the amplitude of 0.03 Å. All displaced configurations generate 3456 components of the Hellmann-Feynman forces. Next, the symmetry of the force constants, following from the *Cmca* space groups, were established and 860 independent parameters of so-called cummulant force constants were fitted to these forces by the singular value decomposition method.[41] We have found that the force constant parameters diminish two order-of-magnitude, or better, in the distance: supercell center-supercell surface. This provides reasonably phonon frequencies at all wave vectors. The force constants were used to construct the dynamical matrix, to diagonalize it and find the phonon frequencies. According to the direct method exact phonon frequencies are obtained at Γ and Y high-symmetry points.

IV. RESULTS

A. Structural investigations

The typical XRD pattern of a 3000-Å-thick β-$^{57}FeSi_2$ film is shown in Fig. 1(a). All peaks in the diffraction pattern could be identified with the powder diffraction data of β-$FeSi_2$,[42] and no other phases except the Si substrate could be detected. Since most diffraction lines of β-$^{57}FeSi_2$ are observed in Fig. 1(a), the film is polycrystalline. This agrees with the results of Ref. 39. The comparison of peak intensities with those given by powder diffraction files may give information about the film texture. The most prominent peak at $2\Theta=29.14$ deg in Fig. 1(a) originates from (220) and (202) reflections of β-$^{57}FeSi_2$, which cannot be resolved. In case of high-quality epitaxial β-$FeSi_2$ layers on Si(100) only this peak should exist.[32] The intensity ratio $I_{(202)/(220)}/I_{(422)}$ of the strongest (202)/(220) peak and the relatively strong (422) peak is measured to be 1.75 for the β-$FeSi_2$ film, while it is known to be only 1.06 for a randomly oriented powder sample. This difference between these values of ~40% is significant and indicates that a crystallographic (202)/(220) texture exists in our β-$^{57}FeSi_2$ films. This conclusion is corroborated by the quadrupole-split doublets observed in the CEM spectra of our β-$FeSi_2$ films, which are asymmetric in the line intensities (see later). The lattice parameters of the β-$FeSi_2$ film deduced from Fig. 1(a) are $a=9.89(6)$ Å, $b=7.81(3)$ Å, and $c=7.82(5)$ Å, in agreement with literature reports[43,44] and the calculated values.

The typical CEM spectrum of a crystalline β-$^{57}FeSi_2$ layer at RT is shown in Fig. 2(a). The spectrum can be de-

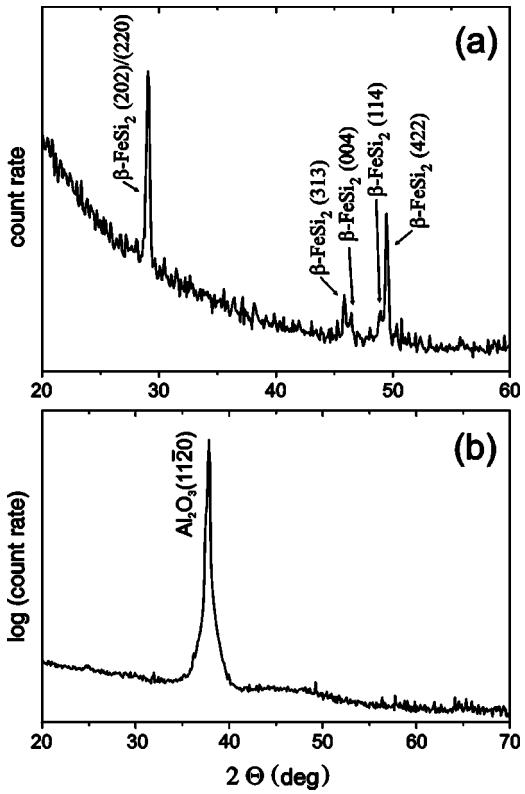

FIG. 1. θ-2θ high-angle x-ray diffraction patterns (Cu K_α radiation) measured at room temperature on the 3000-Å-thick crystalline β-$^{57}FeSi_2$-layer on a Si(100) substrate (a), and the 3000-Å-thick amorphous a-$FeSi_2$-layer on a $Al_2O_3(11\bar{2}0)$ substrate (b).

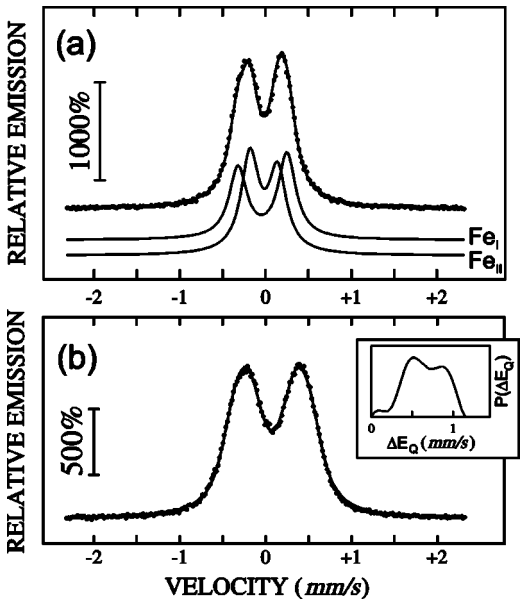

FIG. 2. Mössbauer (CEM) spectra measured at room temperature on the 3000-Å-thick crystalline β-$^{57}FeSi_2$-layer (a), and the 3000-Å-thick amorphous $FeSi_2$-layer (b). The spectrum in (a) is decomposed in a quadrupole-split doublet for the Fe_I site and a doublet for the Fe_{II} site. The spectrum in (b) is described by a distribution $P(\Delta E_Q)$ of quadrupole splittings ΔE_Q (inset).

scribed by two superimposed asymmetric quadrupole doublets with Lorentzian lines, originating from the two different Fe lattice sites (Fe_I and Fe_{II}) in β-$FeSi_2$. The spectral parameters obtained from the least-squares fit of the experimental spectra are as follows: isomer shift $\delta_1 = 0.071(3)$ mm/s and quadrupole splitting $|\Delta E_{Q1}| = 0.57(1)$ mm/s for doublet 1 (Fe_I-site), and $\delta_2 = 0.086(3)$ mm/s and $|\Delta E_{Q2}| = 0.32(1)$ mm/s for doublet 2 (Fe_{II}-site). The FWHM was found to be $\Gamma = 0.25(3)$ mm/s for both doublets. These hyperfine parameters are in good agreement with values from the literature,[45] where it was found that $\Delta E_{Q1} > 0$ and $\Delta E_{Q2} < 0$. We observe an asymmetry in the line intensities of each quadrupole doublet. The ratio of the intensities of the left line (I_1) to the right line (I_2) is found to be $I_1/I_2 = 1.19(8)$ for doublet 1, and $I_1/I_2 = 0.83(7)$ for doublet 2. In case of a polycrystalline material with random orientation of crystallites (i.e., with random orientation of the axes of the electric field gradient (EFG) tensor, the intensity ratio $I_1/I_2 = 1$ is expected, i.e., no asymmetry in the doublet line intensities. The observed value of $I_1/I_2 \neq 1$ are qualitatively explained by a preferred orientation of the main component (V_{zz}) of the EFG tensor due to crystallographic texture, as is also suggested by our XRD results mentioned above. The relative spectral contribution (relative spectral area) of doublet 1 and doublet 2 are found to be 46.6% and 53.4%, respectively (relative to the total spectral area). This could mean that 46.6% of the ^{57}Fe atoms in the β-$FeSi_2$ film occupy Fe_I sites and 53.4% occupy Fe_{II} sites, if equal Lamb-Mössbauer ($f-$) factors are assumed for both Fe sites. In the ideal β-$FeSi_2$ structure both Fe sites are equally populated. The small difference in site occupancy observed for the β-$^{57}FeSi_2$ film may be due to Fe_I site vacancies or antisite Si atoms. Fe vacancies have been inferred also from IR measurements.[43]

Figure 1(b) exhibits the XRD pattern of a 3000-Å-thick amorphous $^{57}FeSi_2$ film on sapphire. Only the $(11\bar{2}0)$ reflection of the Al_2O_3 substrate (and no other Bragg peaks) are observed. This demonstrates the amorphous structure of this $^{57}FeSi_2$ film. Moreover, the CEM spectrum of this a-$^{57}FeSi_2$ film [Fig. 2(b)] is clearly different from that of crystalline β-$^{57}FeSi_2$ [Fig. 2(a)] in that the apparent quadrupole splitting and linewidth are larger for a-$^{57}FeSi_2$. A best fit to the experimental spectrum was obtained by assuming a distribution $P(\Delta E_Q)$ of electric quadrupole splittings ΔE_Q, which is caused by a distribution of local environments in the neighborhood of ^{57}Fe atoms. The result for $P(\Delta E_Q)$ is shown in Fig. 2(b) (right-hand side). A wide range of ΔE_Q values (from 0 to 1.2 mm/s) is observed, which arises from the large electric field gradients induced by the asymmetrical and distorted local atomic arrangements in the amorphous structure, combined with different local near-neighbour configurations. The average value of the magnitude of the quadrupole splitting and of the isomer shift are found to be $\langle \Delta E_Q \rangle = 0.653(1)$ mm/s and $\langle \delta \rangle = +0.181(1)$ mm/s, respectively. These values are in good agreement with corresponding literature values reported for vapor-quenched amorphous thin films ($Fe_{30}Si_{70}$: $\langle \Delta E_Q \rangle \sim 0.6$ mm/s,[46] $FeSi_2$: $\langle \delta \rangle = +0.21$ mm/s[47]). Summarizing, our XRD and CEMS analysis provides convincing evidence of the amorphous nature of our quench-condensed $^{57}FeSi_2$ thin films.

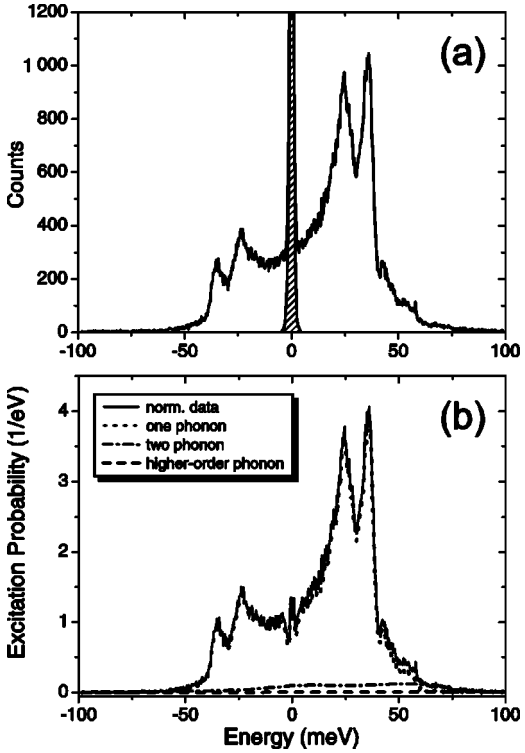

FIG. 3. (a) NRIXS spectrum (raw data) of the 3000-Å-thick crystalline β-$FeSi_2$ layer measured at room temperature, demonstrating phonon annihilation ($E<0$) and phonon creation ($E>0$). Also shown is the instrumental resolution function with FWHM =1 meV (hatched area). The number of counts in the maximum of the central elastic peak is 14869. (b) Decomposition of the NRIX spectrum of the crystalline β-$FeSi_2$ layer shown in (a), after subtraction of the central elastic peak and normalization, in a one-phonon (dotted line), a two-phonon (dashed-dotted line), and higher-order phonon (dashed line) contribution.

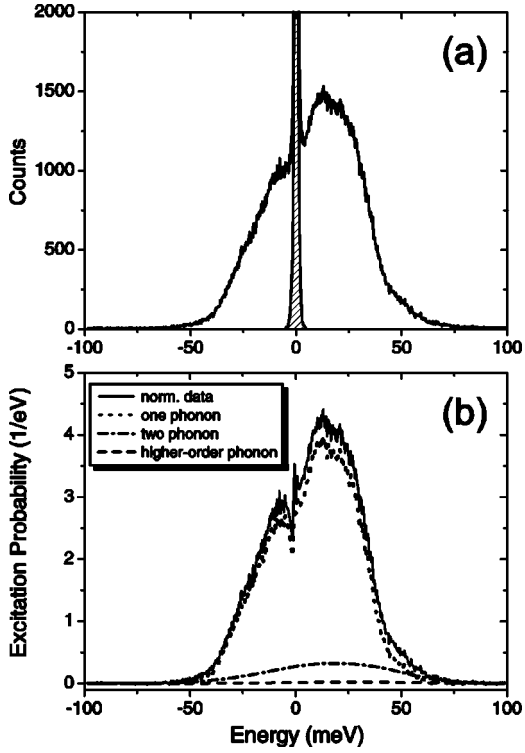

FIG. 4. (a) NRIXS spectrum (raw data) of the amorphous $FeSi_2$ layer measured at room temperature, demonstrating phonon annihilation ($E<0$) and phonon creation ($E>0$). Also shown is the instrumental resolution function with FWHM=1 meV (hatched area). The number of counts in the maximum of the central elastic peak is 20347. (b) Decomposition of the NRIX spectrum of the amorphous $FeSi_2$ layer shown in (a), after subtraction of the central elastic peak and normalization, in a one-phonon (dotted line), a two-phonon (dashed-dotted line), and higher-order phonon (dashed line) contribution.

B. NRIXS study

Figure 3(a) exhibits the NRIXS spectra (excitation probability versus energy transfer E) of crystalline β-$FeSi_2$ measured at RT. The spectrum shows a dominant central elastic peak at the nuclear transition energy E_0 (energy transfer $E=0$ meV) and sidebands at lower and higher energy. X rays with less energy than E_0 excite the nuclear resonance by net annihilation of vibrational quanta (low-energy sideband). The high-energy sideband is produced by creation of vibrational quanta. The observed asymmetry in the spectra reflects the "detailed balance"[48] due to the Boltzmann factor. The instrumental resolution function with a FWHM of 1 meV is also depicted in Fig. 3(a). The resolution function is nearly symmetrical and falls off rapidly from the center without having extended wings. After subtraction of the central elastic peak from the measured NRIXS spectrum the data were normalized according to standard procedures[22,25,35] yielding the vibrational excitation probability per unit energy, $W(E)$. By integration of $W(E)$ over all energies the quantity $(1-f)$ is obtained in a model independent way,[35] where f is the Lamb-Mössbauer factor (or f-factor). The Lamb-Mössbauer factor at RT for crystalline β-$FeSi_2$ was found to be 0.8550. The fraction of the inelastic processes consists of 92.4% one-phonon processes, 7.2% two-phonon processes, and 0.4% multiphonon-processes [Fig. 3(b)]. The partial VDOS [$g(E)$], was deduced from the measured vibrational excitation probability density according to standard procedures.[22,25,35] Figure 5(a) exhibits $g(E)$ of crystalline β-$FeSi_2$. $g(E)$ extends to $\sim$60 meV and exhibits a Debye-like behavior [$g(E)\propto E^2$ for $E\rightarrow 0$] below 15 meV. At $\sim$25 and $\sim$36 meV two strong maxima are observed, the second one being more distinct. Between $\sim$42 and $\sim$58 meV more maxima with less intensity are present, e.g., at $\sim$43 and $\sim$53 meV.

The NRIXS spectrum of amorphous $FeSi_2$ [Fig. 4(a)], measured at RT, is found to be dissimilar to that of the crystalline β-$FeSi_2$-phase [Fig. 3(a)]. The spectrum also shows a dominant central elastic peak at the nuclear transition energy E_0 and sidebands at lower and higher energy. The FWHM of the instrumental resolution function was again 1 meV. After subtraction of the central elastic peak and normalization, the spectrum was decomposed into one-, two- and higher-order-phonon contributions [Fig. 4(b)]. The fraction of the one-phonon contribution was found to be 88.1%, that of the two-phonon contribution is 11.0% and the fraction of the higher-order-phonon contributions is 0.9%. The Lamb-Mössbauer factor at RT for a-$FeSi_2$ was observed to be 0.7814, which is smaller than the corresponding value for β-$FeSi_2$ (Table I).

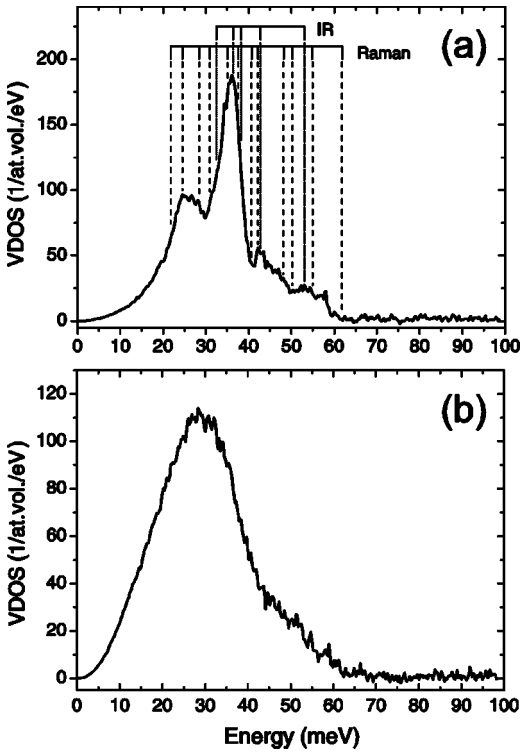

FIG. 5. (a) Partial VDOS, $g(E)$, of the crystalline β-$FeSi_2$ layer at room temperature. Also shown (bar diagrams) are the positions of IR- and Raman-active peaks based on IR and Raman measurements from the literature [see Refs. 43, 49, 51, and 52]. (b) Partial VDOS, $g(E)$, of the amorphous $FeSi_2$ layer at room temperature.

The partial VDOS deduced from the measured vibrational excitation probability density[22,25,35] is shown in Fig. 5(b). The VDOS represents a structureless broad feature, as anticipated for a structurally and atomically disordered material,

TABLE I. Thermal and elastic properties of crystalline β-$FeSi_2$ and amorphous $FeSi_2$ derived from the NRIXS results. The values at $T=0$ K were calculated from the room temperature values. The Debye energy $E_D=k_B\Theta_D$ (Θ_D=Debye temperature) was calculated from the f-factor at room temperature.

	β-$FeSi_2$ crystalline	$FeSi_2$ amorphous
f-factor at RT	0.8550(4)	0.7814(3)
f-factor at 0 K	0.9366(2)	0.9244(1)
Mean atomic force constant $V(\vec{s})$ (N/m)	288(3)	237(2)
Mean kinetic energy $T(\vec{s})$ at RT (meV/atom)	14.95(6)	14.60(5)
Mean kinetic energy $T(\vec{s})$ at 0 K (meV/atom)	8.57(5)	7.63(4)
Vibrational specific heat at RT (k_B/atom)	2.572(8)	2.643(7)
Vibrational entropy at RT (k_B/atom)	2.569(7)	2.962(6)
Debye energy E_D (meV) (calc.)	45.35(7)	35.59(3)

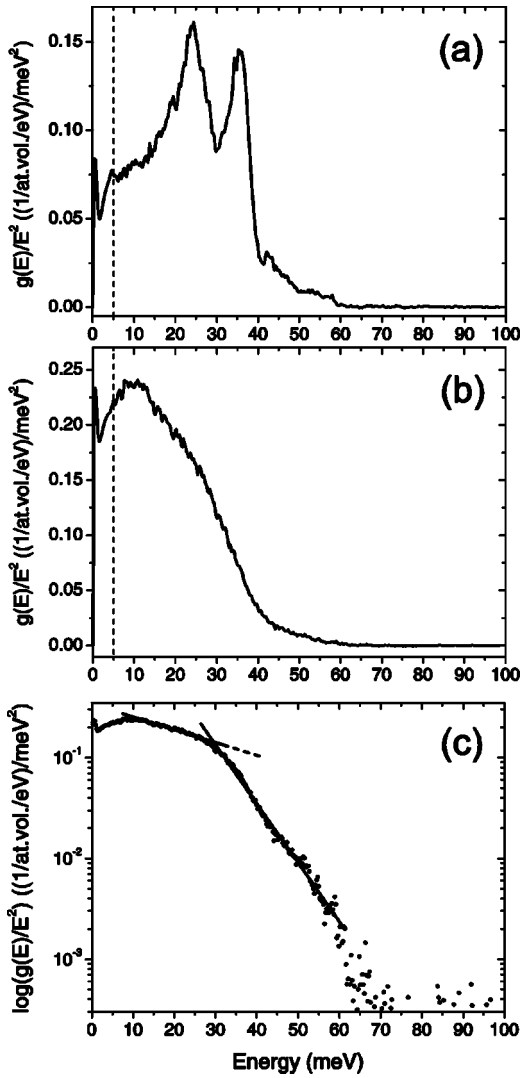

FIG. 6. Reduced partial vibrational density of states, $g(E)/E^2$, vs excitation energy E of the crystalline β-$FeSi_2$ layer at room temperature (a) and the amorphous FeSi layer (b). (The data below 5 meV contain artifacts of the subtraction of the central elastic peak.) (c) plot of $\log[g(E)/E^2]$ vs E of a-$FeSi_2$; the straight lines are least-squares fits to the data.

where van Hove singularities are smeared out. The low-energy modes in $g(E)$ below $\sim$15 meV in Fig. 5(b) are of particular interest because of the boson peak phenomenon.[11–18] The usual way to observe a deviation from Debye-like behavior is to plot the reduced VDOS, $g(E)/E^2$, vs E. In this representation strict Debye-like behavior is reflected by a horizontal line which intersects the $g(E)/E^2$ axis at a value that is proportional to c_S^{-3} (c_S=average sound velocity).[25] Figure 6 shows a plot of $g(E)/E^2$ vs E. Crystalline β-$FeSi_2$ approaches Debye-like behavior below $\sim$15 meV [Fig. 6(a)], while for the amorphous $FeSi_2$ layer a striking and unambiguous rise in $g(E)/E^2$ with a maximum at energy $E_{bp}\sim 10$ meV is observed [Fig. 6(b)].

Further, the Lamb-Mössbauer factor (f-factor), the mean kinetic energy per atom and the mean atomic force constant along the beam direction $\vec{s}$, and the vibrational entropy per atom for amorphous and crystalline β-$FeSi_2$ were

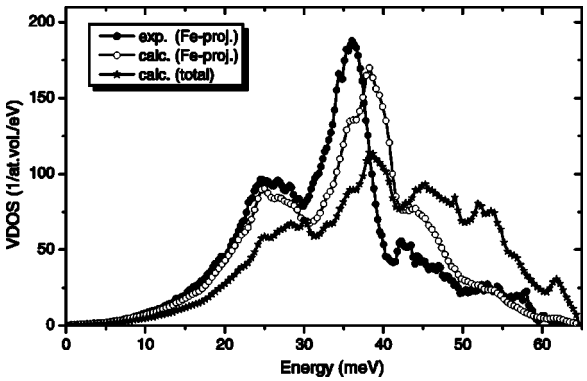

FIG. 7. Fe-projected VDOS of β-$FeSi_2$: Experiment results (●) and results from first-principles calculations (○). Also shown is the calculated total VDOS (⋆). The theoretical Fe-projected and total VDOS include Gaussian smoothing(performed by standard convolution methods) with a width of 1 meV, corresponding to the instrumental resolution of the experiment. The areas below the calculated Fe-projected and calculated total VDOS have been set equal to the area of the experimental Fe-projected VDOS.

obtained from the respective measured VDOS distributions by using the computer program PHOENIX[35] (Table I). These values are given in Table I, together with the calculated Debye energy E_D.

C. Theoretical results

Figure 7 shows the calculated Fe-projected and total VDOS of crystalline β-$FeSi_2$, together with the experimental result. The areas below the calculated Fe-projected and calculated total VDOS have been set equal to the area of the experimental Fe-projected VDOS. For better comparison with the experimental data we have used Gaussian smoothing for the theoretical Fe-projected and total VDOS with a smearing parameter of 1 meV, which corresponds to the instrumental resolution of the experiment. The smoothing was performed by using standard convolution procedures. The calculated Fe-projected VDOS in Fig. 7 shows a dominating peak at 38 meV and less intense sidebands centered near ~25 meV (low energy band), and ~45 and ~54 meV (high energy band). The physics related to these features can be understood from a simple analysis of the crystal structure of β-$FeSi_2$. We used the "Phonon" software[40] which allowed us to visualize the phonon modes directly. The projection of the crystal structure of β-$FeSi_2$ onto the (100) plane is schematically shown in Fig. 8. Vibrations of the whole structure shown in Fig. 8 have been analyzed with respect to the nearest neighbor coordination in order to see dynamical trends when going from low to high phonon energies. However, we noticed that all vibrations are determined by the behavior of tetrahedrally coordinated bonding of each Si atom to its four nearest Fe atoms.

In this way we could determine that the first low-energy band in the VDOS centered near ~25 meV corresponds to angular vibrations of the tetrahedral structure as shown schematically in Figs. 9(a) and 9(b). The dominant second peak of the VDOS (centered at ~38 meV) originates from radial

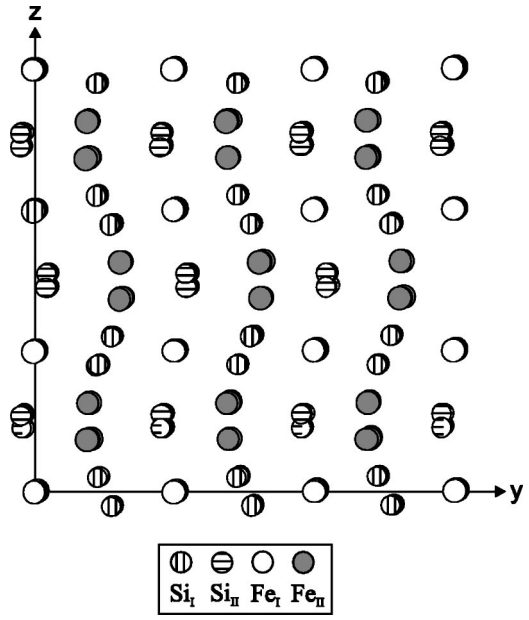

FIG. 8. Projection of the β-$FeSi_2$ structure onto the (100) plane (schematically). The different symbols indicate Si_I, Si_{II}, Fe_I, and Fe_{II} atomic sites, respectively.

distortions, as shown in Fig. 9(c). The high-energy band above ~40 meV does not show a clear difference in the vibrations as compared to the dominant peak. We assume that it arises as a satellite band due to the growing contribution of the Si vibrations with increasing energy. The lighter Si atoms contribute mostly at higher energies, while the Fe atoms determine the vibrational behavior in the lower-energy part of the spectrum.

V. DISCUSSION

As to the best of our knowledge the partial vibrational density of states of crystalline β-$FeSi_2$ and amorphous $FeSi_2$ has not been determined, neither experimentally nor theoretically, in the following the measured VDOS of crystalline β-$FeSi_2$ is compared with literature reports based on IR and Raman measurements.[43,49–52] Further, we compare the measured VDOS with the VDOS of crystalline β-$FeSi_2$ com-

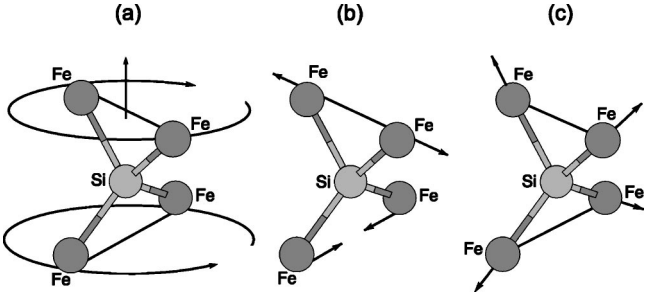

FIG. 9. Tetrahedrally-coordinated bonding environment of the Si atoms in the structure of β-$FeSi_2$. The total number of vibrational modes existing in β-$FeSi_2$ can be approximately decomposed into three simple vibrations of Fe atoms: (a) angular-twist, (b) angular-flap, and (c) radial distortion of the tetrahedral structure.

puted by the density functional theory and direct method.[39,40] The measured VDOS of amorphous *a*-$FeSi_2$ is discussed in terms of the VDOS of amorphous pure Si reported in the literature,[15,16,53,54] and in terms of recent theoretical work on the VDOS in amorphous structures.[20]

A. Crystalline β-$FeSi_2$

According to Dusausoy *et al.*[55] β-$FeSi_2$ crystallizes in the orthorhombic space group *Cmca*-D_{2h}^{18} with 48 atoms per unit cell. The projection of the crystallographic structure onto the (100) plane is shown in Fig. 8. In this structure two different Fe sites (Fe_I, Fe_{II}) and two different Si sites (Si_I, Si_{II}) exist. Factor group analysis yields nine IR- and twelve Raman-active vibrational modes for each Si_I and Si_{II} site and five IR- and six Raman-active vibrational modes for each Fe_I and Fe_{II} site.[43,56] Each Fe site has 4 Si_I and 4 Si_{II} atoms as nearest neighbors. The interatomic Fe-Si distances lie between 2.34 and 2.39 Å for Fe_I, and between 2.34 and 2.44 Å for Fe_{II}. From this fact the conclusion can be drawn that the two Fe sites are almost similar, and that the bounds of vibrational frequencies of the Fe modes of each site will be very close to each other and perhaps overlap. As the crystallographic unit cell of β-$FeSi_2$ has a symmetry center, group theory forbids the IR-active mode to be Raman-active and vice versa, so that the IR and the Raman peaks cannot occur at the same frequencies.[43]

The IR spectra of polycrystalline and single-crystalline β-$FeSi_2$ exhibit five broadened main peaks, resulting from the five IR-active modes of the Fe_I and Fe_{II} site which lie close together. These five broadened peaks are located at average energies of 32.5 (peak1), 36.4 (peak2), 38.3 (peak3), 42.8 (peak4), and 53.1(peak5) meV.[43,49–52] They are indicated in the bar diagram in Fig. 5(a). Depending on the structural quality of the β-$FeSi_2$ layers, the positions of the IR peaks can slightly deviate up to 2 meV from each other. In all these spectra peak3 has the highest intensity. Therefore, the main peak of the experimental β-$FeSi_2$ VDOS at ~36 meV [Fig. 5(a)] is correlated with IR peak2 and peak3. The weak shoulder near ~32 meV in the experimental VDOS is related to IR peak1. The shoulder near 43 meV on the right-hand side of the main peak can be asssigned to IR peak4. IR peak5 (with the weakest IR intensity) appears in the VDOS as a weak bump at ~53 meV. Thus, all peaks of the IR-active internal modes determined by infrared measurements are observed in the experimental VDOS. Moreover, the relative peak intensities obtained by the two methods show qualitatively good agreement.[43,49–52]

Aside from the ten IR-active modes, most of the expected 12 Raman-active modes can be observed in the VDOS [Fig. 5(a)]. Raman spectra exhibit a peak of highest intensity at an energy of ~30.9 meV.[43,49–51] This peak (together with the IR-active peak1) may be associated with the weak shoulder near ~32 meV in the steeply rising left part of the dominant VDOS peak [Fig. 5(a)]. The other eleven Raman peaks are more or less clearly reflected in the VDOS. Their positions are 21.8, 24.5, 28.4, 35.1, 37.6, 40.7, 42.2, 48.2, 50.2, 54.9, and 61.9 meV[49,43] as indicated by the bar diagram in Fig. 5(a). The broadband centered near ~25 meV in the VDOS is associated with the three Raman peaks at 21.8, 24.5, and 28.4 meV. Summarizing, the main peak at ~36 meV in the VDOS is correlated with two IR- and two Raman-active peaks, whereas the second strongest band centered near ~25 meV in the VDOS is associated with three Raman-active modes.

We notice in Fig. 7 that good agreement between the experimental and computed VDOS is obtained up to about 28 meV, while there is a systematic shift to higher energies of the theoretical partial VDOS for energies larger than ~28 meV. Our theoretical analysis shows that for β-$FeSi_2$ the separation of the vibrations into angular and radial parts is important. The high-frequency part of the calculated Fe-projected VDOS is shifted towards higher values. This shift is still within a typical accuracy of the method. It can be caused by a slightly smaller calculated lattice constant *a*, anharmonic contributions, or by the fact that our *ab initio* calculations slightly overestimate interatomic bond strengths. This gives a constant frequency shift in comparison to the experimental result. In the weaker band near ~25 meV we do not see this shift, which means that below 28 meV the atomic bonds between Si and Fe remain about unchanged. However, above ~28 meV 28 meV the energy is large enough to activate the radial bonding vibrations between Si and Fe atoms. This gives rise to the dominant peak at ~36 meV in the experiment (at ~38 meV in the calculation), which involves all possible distortions shown in Fig. 9.

B. Amorphous $FeSi_2$

The VDOS of amorphous $FeSi_2$ [Fig. 5(b)] is distinctly different from the VDOS of crystalline β-$FeSi_2$ [Fig. 5(a)]. While the crystalline VDOS shows a pronounced peak and weaker side bands, the amorphous VDOS consists of an almost structureless broad band with a peak at ~30 meV. However, a shoulder can be observed between ~40 and 60 meV in the amorphous VDOS, which is reminescent of the weak third band in the same energy range in the VDOS of crystalline β-$FeSi_2$ [Fig. 5(a)]. These higher energy vibrations are related to the vibrational behavior of the light Si atoms, which appears to be similar in the crystalline and amorphous structure. Amorphous $FeSi_2$ exhibits a deviation from Debye-like behavior at low energies.The latter becomes clear in the plot of the reduced VDOS [$g(E)/E^2$ vs E] [Fig. 6(b)], where a strong peak at ~10 meV can be observed, which is absent in the crystalline counterpart. Therefore, we identify this 10 meV peak as boson peak of *a*-$FeSi_2$. Notice that the boson peak is located at an energy E, which is much smaller than the lowest phonon peak energy in the VDOS of crystalline β-$FeSi_2$ of ~25 meV, or smaller than the lowest Raman energy of ~22 meV. Obviously the boson peak energy (~10 meV) is observed to lie at excitation energies much lower than any phonon peaks of crystalline β-$FeSi_2$, and is within the energy range of the Debye behavior of crystalline β-$FeSi_2$.

Within the first 25 meV the VDOS of crystalline β-$FeSi_2$ and amorphous $FeSi_2$ show reasonable agreement with the VDOS distributions of crystalline and amorphous Si, respectively. The latter have been measured by means of

inelastic neutron scattering by Kamitakahara *et al.*[54] and calculated in the harmonic approximation by Finkemeier *et al.*[15,16] Crystalline Si (*c*-Si), like crystalline β-$FeSi_2$, exhibits no boson peak, whereas amorphous Si (*a*-Si), like amorphous $FeSi_2$, shows a boson peak. The TA peak in the VDOS of *c*-Si is located at ~20 meV.[15,16,54] The calculations of Finkemeier *et al.*[15,16] revealed that the TA peak of Si, together with the boson peak, shifts toward lower energies with increasing degree of atomic disorder (Si with an amorphous volume fraction of 28% has a boson peak at an calculated energy of ~5 meV). This behavior was experimentally confirmed by Laermans *et al.*[53] Using Raman spectroscopy they investigated Si disordered by irradiation with neutrons, which, however, leads to an amorphous volume fraction of only 4%. The observed boson peak was located at 14.1 meV. The experimental data of Kamitakahara *et al.*[54] provide a boson peak for *a*-Si between 10 and 15 meV.

The boson peak of amorphous $FeSi_2$ is located at ~10 meV [Fig. 6(b)], which is within the energy range where the boson peak of *a*-Si was observed. However, in comparison with *a*-Si the boson peak of amorphous $FeSi_2$ is clearly broadened. According to Finkemeier *et al.*[15,16] the boson peak of *a*-Si is a direct result of a shift and a broadening of the TA peak. This agrees in part with the model calculations by Schirmacher *et al.*[17,18] They observed a boson peak by introducing structural disorder into a harmonic model. But the appearance of extra states in the low-energy part of the VDOS seems to be caused only by a broadening and not by a shift of the VDOS in their calculations. The observed maximum in the partial VDOS of amorphous $FeSi_2$ at ~30 meV [Fig. 5(b)] is located close to the peak position of the low-energy band at ~27 meV of crystalline β-$FeSi_2$ [Fig. 5(a)]. In the amorphous state this peak clearly broadens (but is not shifted to smaller energies), while the dominant peak of crystalline β-$FeSi_2$ near 36 meV has vanished in the amorphous state. Because of this broadening, no Debye-like behavior in the low-energy range is observed. Thus, the model of Schirmacher *et al.*[17,18] appears to be appropriate to explain qualitatively the occurrence of the boson peak in amorphous $FeSi_2$. In the range between about 40 and 60 meV the VDOS of *a*-$FeSi_2$ exhibits several smaller peaks similar to the β-$FeSi_2$ case. This indicates that in this energy range some of the vibrational properties of the crystalline state (vibrations of Si atoms) are retained in the amorphous state.

Recently, the NRIXS technique has been successfully employed by Chumakov *et al.*[20] to measure the boson peak via ^{57}Fe-containing ferrocene probe molecules embedded in various organic glass matrices. Based on experiments and calculations, these authors showed that at energies above the boson peak the reduced density of states exhibits a universal exponential decrease,[20] i.e., $g(E)/E^2 \propto \exp(-E/E_0)$, with a parameter it E_0 close to the boson peak energy, E_{bp}. In Fig. 6(c) we have plotted $\log[g(E)/E^2]$ vs E, as measured on our amorphous $FeSi_2$ film. As can be seen in Fig. 6(c), directly above the boson peak, i.e., in the range $\sim 13\ \text{meV} \leqslant E \leqslant \sim 25$ meV, the experimental data follow an exponential. From a straight-line fit [Fig. 6(c)] a value of 34.3 meV is obtained for the parameter E_0, which, however, is much larger than the boson peak energy of ~10 meV, and, therefore, seems to be at variance with the prediction of Ref. 20. Surprisingly, however, the data in Fig. 6(c) can be reasonably well described by an exponential behavior (straight line over two decades) in the high-energy range of $\sim 30\ \text{meV} \leqslant E \leqslant \sim 60$ meV. The straight-line fit in this energy range results in a value of 7.4 meV for the parameter E_0, which is close to the boson-peak energy (~10 meV), and apparently agrees with the universal exponential behavior calculated and observed in Ref. 20.

VI. SUMMARY

The Fe-projected partial VDOS, $g(E)$, of crystalline β-$^{57}FeSi_2$ and amorphous $^{57}FeSi_2$ thin films has been measured by NRIXS of 14.4125 keV synchrotron radiation. The VDOS of β-$^{57}FeSi_2$ exhibits characteristic features that coincide with the energy of prominent IR and Raman spectral lines reported in the literature.[43,49–52]. The VDOS of β-$FeSi_2$ was computed by using the density functional theory combined with the direct method. The characteristic features in the experimental VDOS are well reproduced in the theoretical VDOS. Contrary to the VDOS of crystalline β-$FeSi_2$, which approaches a Debye-like behavior at low phonon energies, the VDOS of amorphous $^{57}FeSi_2$ reveals vibrational excitations in excess of Debye-like behavior. These excess excitations are reflected in the boson peak, observed at ~10 meV in the reduced density of states, $g(E)/E^2$. Well above the boson peak, in the energy range $\sim 30\ \text{meV} \leqslant E \leqslant 60$ meV, $g(E)/E^2$ is found to be approximately $\propto \exp(E/E_0)$ over two decades, as predicted and observed recently by Chumakov *et al.*[20] Finally, our work demonstrates that NRIXS of synchrotron radiation is a unique method for the measurement of the VDOS of crystalline and amorphous thin film systems.

ACKNOWLEDGMENTS

We are grateful to U. v. Hörsten (Duisburg) for valuable technical assistance. Work at Duisburg was supported by Deutsche Forschungsgemeinschaft (GRK 277 and Ke 273/17-1). Work at Argonne was supported by the US Department of Energy, Basic Energy Sciences, Office of Science, under Contract No. W-31-109-Eng-38.

*Author to whom correspondence should be addressed. Email address: Keune@uni-duisburg.de

[1] H. Lange, Phys. Status Solidi B **201**, 3 (1997).
[2] M. C. Bost and J. E. Mahan, J. Appl. Phys. **64**, 2034 (1998).
[3] E. Arushanov, E. Bucher, Ch. Kloc, O. Kulikova, L. Kulyuk, and A. Siminel, Phys. Rev. B **52**, 20 (1995).
[4] D. Leong, M. Harry, K. J. Reeson, and K. P. Homewood, Nature (London) **387**, 686 (1997).
[5] M. Milosavljević, G. Shao, N. Bibić, C. N. McKinty, C. Jeynes, and K. P. Homewood, Appl. Phys. Lett. **79**, 1438 (2001).
[6] S. Sanguinetti, C. Calegari, V. R. Velasco, G. Benedek, F. Tavazza, and L. Miglio, Phys. Rev. B **54**, 9196 (1996).
[7] H. von Känel, R. Stalder, H. Sirringhaus, N. Onda, and J. Henz, Appl. Surf. Sci. **53**, 196 (1991).
[8] A. L. Vazquez de Parga, J. De la Figuera, C. Ocal, and R. Miranda, Europhys. Lett. **18**, 595 (1992).
[9] Le Tanh Vinh, J. Chevrier, and J. Derrien, Phys. Rev. B **46**, 15 946 (1992).
[10] H. Ch. Schaefer, B. Roesen, H. Moritz, A. Rizzi, B. Lengeler, H. Lüth, and D. Gerthsen, Appl. Phys. Lett. **62**, 2271 (1993).
[11] *Amorphous Solids—Low Temperature Properties*, edited by W. A. Phillips (Springer, Berlin, 1981).
[12] *Dynamics of Disordered Materials II*, edited by A. J. Dianoux, W. Petry, and D. Richter (North-Holland, Amsterdam, 1993).
[13] V. K. Malinkovsky, V. N. Novikov, P. P. Parshin, A. P. Sokolov, and M. G. Zemlyanov, Europhys. Lett. **11**, 43 (1990).
[14] H.-B. Suck and H. Rodin, in *Glassy Metals II*, Topics in Applied Physics Vol. 53, edited by H. Beck and H.-J. Güntherodt (Springer, Berlin, 1983), p. 217.
[15] F. Finkemeier and W. von Niessen, Phys. Rev. B **63**, 235204 (2001).
[16] F. Finkemeier and W. von Niessen, Phys. Rev. B **66**, 087202 (2002).
[17] W. Schirmacher, G. Diezemann, and C. Ganter, Phys. Rev. Lett. **81**, 136 (1998).
[18] W. Schirmacher, G. Diezemann, and C. Ganter, Physica B **263–264**, 160 (1999).
[19] E. Maurer and W. Schirmacher, J. Low Temp. Phys. **137**, 453 (2004).
[20] A. I. Chumakov, I. Sergueev, U. van Bürck, W. Schirmacher, T. Asthalter, R. Rüffer, O. Leupold, and W. Petry, Phys. Rev. Lett. **92**, 245508 (2004).
[21] M. Seto, Y. Yoda, S. Kikuta, X. W. Zhang, and A. Ando, Phys. Rev. Lett. **74**, 3828 (1995).
[22] W. Sturhahn, T. S. Toellner, E. E. Alp, X. W. Zhang, M. Ando, Y. Yoda, S. Kikuta, M. Seto, C. W. Kimball, and B. Dabrowski, Phys. Rev. Lett. **74**, 3832 (1995).
[23] A. I. Chumakov, R. Rüffer, H. Grünsteudel, H. F. Grünsteudel, G. Grübel, J. Metge, O. Leupold, and H. A. Goodwin, Europhys. Lett. **30**, 427 (1995).
[24] A. I. Chumakov and W. Sturhahn, Hyperfine Interact. **123/124**, 781 (1999).
[25] E. E. Alp, W. Sturhahn and T. S. Toellner, J. Phys.: Condens. Matter **13**, 7645 (2001).
[26] W. Sturhahn, J. Phys.: Condens. Matter **16**, S497 (2004).
[27] B. Roldan Cuenya, W. Keune, W. Sturhahn, T. S. Toellner, and M. Y. Hu, Phys. Rev. B **64**, 235321 (2001).
[28] W. Keune and W. Sturhahn, Hyperfine Interact. **123/124**, 847 (1999).
[29] T. Ruckert, W. Keune, B. Sahoo, W. Sturhahn, T. Toellner, E. E. Alp, and R. Roehlsberger, Hyperfine Interact. **144/145**, 65 (2002).
[30] W. Keune, T. Ruckert, B. Sahoo, W. Sturhahn, T. S. Toellner, E. E. Alp, and R. Röhlsberger, J. Phys.: Condens. Matter **16**, S379 (2004).
[31] A. I. Chumakov and R. Rüffer, Hyperfine Interact. **113**, 59 (1998).
[32] H. Chen, P. Han, X. D. Huang, and Y. D. Zheng, J. Vac. Sci. Technol. A **14**, 905 (1996).
[33] K. M. Geib, J. E. Mahan, R. G. Long, M. Nathan, and G. Bai, J. Appl. Phys. **70**, 1730 (1991).
[34] R. A. Brand, Nucl. Instrum. Methods Phys. Res. B **28**, 398 (1987).
[35] W. Sturhahn, Hyperfine Interact. **125**, 149 (2000).
[36] G. Kresse and J. Furthmüller, Software VASP, Vienna (1999); Phys. Rev. B **54**, 11 169 (1996); Comput. Mater. Sci. **6**, 15 (1996).
[37] G. Kresse and J. Hafner, Phys. Rev. B **47**, 558 (1993); **49**, 14 251 (1994).
[38] D. Vanderbilt, Phys. Rev. B **41**, 7892 (1990).
[39] K. Parlinski, Z. Q. Li, and Y. Kawazoe, Phys. Rev. Lett. **78**, 4063 (1997).
[40] K. Parlinski, PHONON Software, Cracow, Poland, 2003.
[41] K. Parlinski, AIP Conf. Proc. **479**, 121 (1999).
[42] Powder Diffraction File, Card 20-352, Joint Committee on Powder Diffraction Standards, published by International Center for Diffraction Data, 1989.
[43] K. Lefki, P. Muret, E. Bustarret, N. Boutarek, R. Madar, J. Chevrier, J. Derrien, and M. Brunel, Solid State Commun. **80**, 791 (1991).
[44] M. Fanciulli, G. Weyer, H. von Känel, and N. Onda, Phys. Scr., T **T54**, 16 (1994).
[45] H. Reuther, G. Behr, M. Dobler, and A. Teresiak, Hyperfine Interact. **C3**, 385 (1998).
[46] F. E. Fujita, in *Application of Nuclear Techniques to the Studies of Amorphous Metals*, edited by U. Gonser (International Atomic Energy Agency, Vienna, 1981), p. 173.
[47] G. Marchal, Ph. Mangin, M. Piecuch, and Ch. Janot, J. Phys. Colloq. **37**, 763 (1976).
[48] W. Sturhahn and V. G. Kohn, Hyperfine Interact. **123/124**, 367 (1999).
[49] G. Guizetti, F. Marabelli, M. Patrini, Y. Mo, N. Onda, and H. von Känel, Mater. Res. Soc. Symp. Proc. **320**, 127 (1994).
[50] G. Guizetti, F. Marabelli, M. Patrini, P. Pellegrino, B. Pivac, L. Miglio, V. Meregalli, H. Lange, W. Henrion, and V. Tomm, Phys. Rev. B **55**, 14 290 (1997).
[51] G. Fahsold, K. Singer, and A. Pucci, J. Appl. Phys. **91**, 145 (2002).
[52] H. Lange, W. Henrion, B. Selle, G.-U. Reinsperger, G. Oertel, and H. von Känel, Appl. Surf. Sci. **102**, 169 (1996).
[53] C. Laermans and M. Coeck, Physica B **263–264**, 280 (1999).
[54] W. A. Kamitakahara, C. M. Soukoulis, H. R. Shanks, U. Buchenau, and G. S. Grest, Phys. Rev. B **36**, 6539 (1987).
[55] P. Y. Dusausoy, J. Protas, R. Wandji, and B. Roques, Acta Crystallogr., Sect. B: Struct. Crystallogr. Cryst. Chem. **B27**, 1209 (1971).
[56] D. L. Rousseau, R. P. Bauman, and S. P. S. Porto, J. Raman Spectrosc. **10**, 253 (1981).